The Influence of Convective Thermal Forcing on the Three-Dimensional Circulation around Squall Lines

RAJUL E. PANDYA*

National Center for Atmospheric Research,+ Boulder, Colorado

DALE R. DURRAN

Department of Atmospheric Sciences, University of Washington, Seattle, Washington

MORRIS L. WEISMAN

National Center for Atmospheric Research, Boulder, Colorado

(Manuscript received 1 April 1998, in final form 12 March 1999)

ABSTRACT

Midlatitude squall lines are typically trailed by a large region of stratiform cloudiness and precipitation with significant mesoscale flow features, including an ascending front to rear flow; a descending rear inflow jet; line-end vortices; and, at later times, mesoscale convective vortices. The present study suggests that the mesoscale circulation in the trailing stratiform region is primarily determined by the time-mean pattern of heating and cooling in the leading convective line. Analysis of the line-normal circulation shows that it develops as thermally generated gravity waves spread away from the leading line. Midlevel line-end vortices are the result of diabatically driven tilting of horizontal vorticity generated by the time-mean thermal forcing. In the presence of the Coriolis force, a symmetric thermal forcing generates an asymmetric stratiform circulation and a pattern of vertical displacement that resembles the comma-shaped stratiform anvil observed in real systems; this suggests that asymmetries in the cloud and circulation behind midlatitude squall lines are not necessarily the result of asymmetries in the convective leading line.

1. Introduction

Mesoscale convective systems (MCSs) are often organized into squall lines in which a relatively narrow line of strong convective cells is trailed by an extensive region of stratiform precipitation (Houze 1993). Although the contribution from the stratiform region is not insignificant (Braun et al. 1996), the latent heat released by these systems is dominated by the contribution of the leading convective line (Houze 1989; Gallus and Johnson 1991). The present study seeks to build upon the many previous investigations of the mechanisms by which vigorous convection along the leading edge of the squall line influences the circulations that develop in the stratiform region; the thesis of this work is that the three-dimensional circulation around squall lines is primarily generated by the low-frequency component of the latent heating and cooling in the leading convective line.

Past studies of the communication between the leading line and the trailing stratiform region have emphasized the development of the line-normal circulations, including the ascending front to rear flow (FTRF) and the descending rear inflow jet (RIJ) (e.g., Zipser 1977; Houze 1989). Using multiple aircraft observations of a single convective line, LeMone (1983) suggested that a rearward tilt to the convective heating produces a midlevel hydrostatic low beneath and behind the tilted heating, which influences the development of the RIJ and FTRF. Klimowski (1994) suggested, based on dual Doppler analysis of the entire life cycle of a squall line, that the RIJ is primarily a response to the strong convection at the system's leading edge. Lafore and Moncrieff (1989) and Weisman (1992) attributed the development of line-normal circulations in the trailing stratiform region of their two-dimensional numerical simulations to buoyancy perturbations within the convective region.

* Current affiliation: Department of Geology and Astronomy, West Chester University, West Chester, Pennsylvania.

+ The National Center for Atmospheric Research is sponsored by the National Science Foundation.

Corresponding author address: Rajul Pandya, NCAR, P.O. Box 3000, Boulder, CO 80307-3000.
E-mail: rpandya@wcupa.edu

The connection between the leading convective line and the stratiform region has also been explored in a variety of simplified models. Several investigators have considered the linear response of a stably stratified resting fluid to a specified heat source (e.g., Smith and Lin 1982; Lin and Smith 1986; Nicholls et al. 1991; Mapes 1993; Pandya et al. 1993). In the subset of these studies that are particularly relevant to deep convection, Nicholls et al. (1991) and Mapes (1993) considered a thermal forcing with a vertical profile that resembled that of observed mesoscale convective systems; it consisted of both heating and cooling.

Gravity waves clearly play a major role in communicating the thermal forcing to the surrounding environment in these idealized models. The direction of energy propagation for gravity waves in a resting atmosphere can be described by

$$\cot(\alpha) = \frac{\omega}{\sqrt{N^2 - \omega^2}},$$

where α is the angle of energy propagation measured from the vertical, N is the buoyancy frequency, and ω is the frequency of the wave. From this relationship, gravity waves with low frequencies propagate horizontally and would be expected to influence the tropospheric circulations. Indeed, in these simple models, a steady thermal forcing (which projects most directly onto low-frequency gravity waves) produces circulations that are largely confined to the troposphere, even when vertical propagation is allowed (Pandya et al. 1993). It is interesting to note that even in the idealized, linear models, the gravity waves generated by a steady thermal forcing bear little resemblance to the canonical picture of a monochromatic gravity wave. Instead the gravity wave response consists of a relatively compact leading edge that leaves behind a region of disturbed flow (Bretherton and Smolarkiewicz 1989; Nicholls et al. 1991; Mapes 1993; Pandya et al. 1993).

The relevance of these simpler models to real squall line systems has been supported by the appearance of convectively generated gravity waves in numerical simulations by Tripoli and Cotton (1989), Schmidt and Cotton (1990), and Cram et al. (1992). Yang and Houze (1995a) suggested that the radar reflectivity cells in the convective region are manifestations of trapped gravity waves and McAnelly et al. (1997) asserted that convectively generated gravity waves can modulate the strength of convection, producing an initial maximum followed by a decay and a subsequent reintensification.

In spite of the dynamical insight afforded by the simplified models, the idealizations they use preclude realistically representing the wind shear, nonlinearity, and shape and structure of the thermal forcing. Garner and Thorpe (1992) developed a nonlinear model with realistic environmental shear to investigate the relationship between convection and the large-scale circulation. They parameterized their heating and cooling function based on vertical motions in the vicinity of the convective line. Although their parameterized thermal forcing varied in time, ''it eliminated the microphysical and precipitation time scales.'' Garner and Thorpe found that the circulation in the stratiform region developed behind ''storm fronts'' that propagated away from the thermal forcing. They further suggested that the storm fronts' propagation was at least partly the result of linear waves.

Pandya and Durran (1996, hereafter PD96) performed similar simulations using a steady, specified thermal forcing. They constructed their thermal forcing from the time mean of the latent heating and cooling in the convective line of a squall line simulation that used warm-cloud parameterized microphysics. PD96 found that the time-mean forcing produced a circulation trailing the forcing that resembled the circulation in the trailing anvil of the conventional squall line simulation with microphysics as well as the circulation in the trailing anvil of real squall lines. Like Garner and Thorpe (1992), PD96 found that the circulation developed behind outwardly propagating wave fronts. PD96 suggested that these wave fronts and the circulation trailing them were polychromatic gravity waves excited by the thermal forcing, similar to the linear gravity waves in idealized models (e.g., Bretherton and Smolarkiewicz 1989; Nicholls et al. 1991; Mapes 1993; Pandya et al. 1993). PD96 also investigated the sensitivity of the circulation to the shape and structure of the specified thermal forcing; they found that a realistic circulation developed only when the heating and cooling slanted backward with height and when the cooling was shorter than and behind the heating, as in the mature phase of the convective systems with a well-established RIJ, FTRF, and surface cold pool.

While considerable dynamical insight into real squall line systems has been obtained by examining idealized two-dimensional simulations, real squall lines include significant three-dimensional circulations. The three-dimensional features of significance in real squall line systems are illustrated in the conceptual models shown in Fig. 1. Houze et al. (1990) have proposed two general classes of three-dimensional organization for squall lines with trailing stratiform regions: symmetric and asymmetric. In symmetric systems the trailing stratiform region is centered directly behind an arc-shaped leading line, and the midlevel circulation in the stratiform region is dominated by two counterrotating vortices with an RIJ centered between them (Smull and Houze 1985; Smull and Houze 1987; Jorgenson and Smull 1993). These vortices have been referred to as line-end vortices because of their proximity to the ends of the leading line (Skamarock et al. 1994a; Weisman and Davis 1998). In asymmetric systems the stratiform region shifts to the northeast relative to the arc-shaped leading line. Instead of a pair of counterrotating line-end vortices, the midlevel circulation in the trailing stratiform region consists of a single cyclonic vortex referred to as the mesoscale convective vortex (MCV). The strongest RIJ is

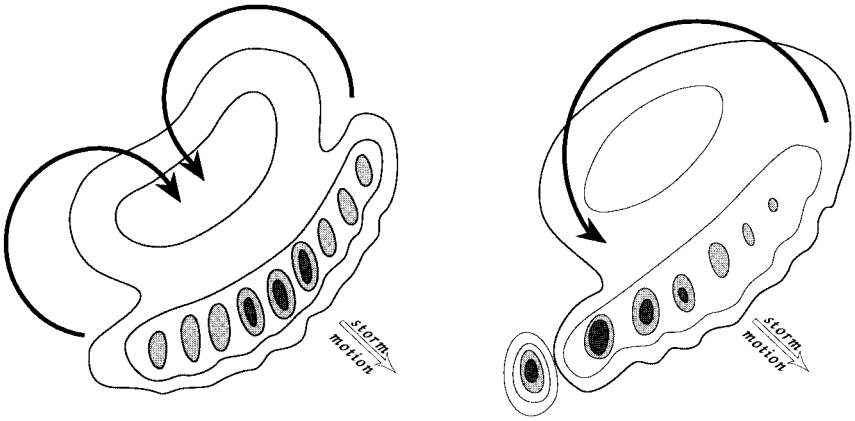

FIG. 1. Conceptual models of two squall line systems: (a) symmetric and (b) asymmetric. Radar reflectivity is indicated by stippling, midlevel circulation by vectors. Adapted from Houze et al. (1990).

often observed at the southern end of the MCV (e.g., Schmidt and Cotton 1989).

Increasing evidence suggests that the symmetric and asymmetric classifications can represent different stages in the life cycle of squall line systems that evolve in the absence of strong large-scale linear forcing. Loehrer and Johnson (1995) and Hilgendorf and Johnson (1998) observed many systems that evolved from symmetric to asymmetric organization. Numerical simulations of three-dimensional squall lines by Skamarock et al. (1994a) and Weisman and Davis (1998) show a similar evolution from symmetric to asymmetric structure, but only when the Coriolis force is included in the governing equations.

In the present work, we seek to investigate the influence of convective thermal forcing in fully three-dimensional squall line systems. Past three-dimensional studies with simple models include Lin (1986) and Lin and Li (1988), who considered the linear response of a stably stratified environment to an isolated, analytic heat source. Using this simple model, they were able to generate upper-level cold anomalies that resembled the v-shaped pattern of cold cloud top above real-world convection. Fulton et al. (1995) considered the response of mass injection between isentropic levels and were able to produce an upper-tropospheric–lower-stratospheric anticyclone that resembled the anticyclones observed above real MCSs. Injection of mass has the same effect as heating in their simplified model (Betherton 1988). Schubert et al. (1989) modeled the long-term influence of the squall line on the large-scale environment in terms of the geostrophic adjustment to an infinite line of steady heating. This study was further idealized in that it was two-dimensional, although it included the influence of the Coriolis force. The potential vorticity anomalies that developed after 8 h were broadly consistent with observations, but the modeled vorticity did not reflect the finite length of real squall lines, lacked the detailed structure of the observations, and did not fully address the three-dimensional circulations.

As in two dimensions, the simple models do not realistically represent the environment or the structure of the thermal forcing in real-world MCSs. In the present work we use nonlinear simulations with environmental shear and steady thermal forcing representative of real squall line systems. We extend the methodology of PD96 to three dimensions and compare the circulations in parallel ''moist'' and ''dry'' simulations. The moist simulation is performed using a standard three-dimensional cloud model, which includes a parameterization of microphysical processes. The dry simulation is identical to the moist simulation, except that the microphysical parameterization is switched off and all motions are generated by a specified thermal forcing. The two-dimensional results of PD96 show strong sensitivity to the specification of the steady thermal forcing. The challenges of specifying a thermal forcing that generates realistic flows in three dimensions are considerably greater than in two dimensions because there is more spatial and temporal variability in the location of the updraft cores. As a severe test of our hypothesis that the low-frequency component of the thermal forcing is primarily responsible for the circulation in the trailing anvil, the three-dimensional dry simulation will use a *steady* thermal forcing constructed from the time-averaged three-dimensional pattern of the latent heat release and absorbed in the moist simulation.

The next section presents a discussion of the numerical models and the initial conditions in the dry and moist simulations. A general comparison of the moist and dry simulations is presented in section 3. Section 4 examines the evolution of the line-normal circulations, and section 5 focuses on the evolution of the line-end vortices. Section 6 investigates the circulation that de-

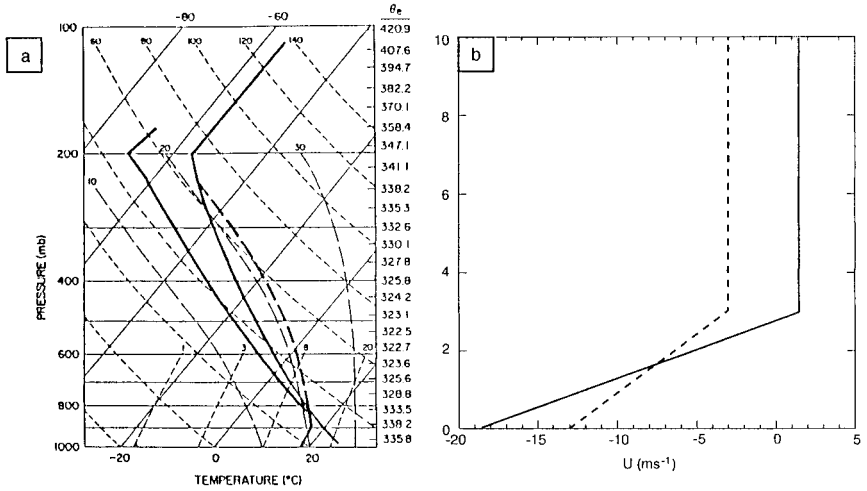

FIG. 2. (a) Skew T diagram of the initial thermodynamic profile. (b) Initial profile of the x component of the storm-relative winds. Dotted line is the weak-shear profile, solid line is the moderate-shear profile.

velops from symmetric thermal forcings in a rotating atmosphere. Conclusions are offered in section 7.

2. Model details

a. Numerical model

The moist simulations are described in Weisman and Davis (1998, hereafter WD98). They were performed using a fully compressible, nonhydrostatic, three-dimensional numerical model (Klemp and Wilhelmson 1978). The horizontal resolution was 2 km in a horizontal domain 600 km on each side. The vertical resolution was 700 m, and the model extended to a height of 17.5 km. Lateral and upper boundaries were open to allow the outward propagation of wave energy. The moist simulations used a warm-cloud microphysical parameterization that did not include ice-phase processes. Although some studies indicate that local ice processes can influence the strength of the circulation in the stratiform region (e.g., Yang and Houze 1995b), realistic circulations still develop in two-dimensional simulations in which ice processes are neglected (e.g., Fovell and Ogura 1988; Weisman 1992). Skamarock et al. (1994b) compared three-dimensional simulations of squall line systems with and without ice microphysics and found that, although the inclusion of ice-microphysical processes did accelerate the evolution of the stratiform anvil and lead to a larger region of stratiform precipitation, the simulations with and without ice microphysics were dynamically very similar. Further, the latent heat release and absorption in the convective line is dominated by the liquid–vapor transition (Houze 1989). Since the goal of the present study is to investigate the influence of the thermal forcing of the convective region, we can neglect ice processes.

The dry simulations are performed with a modified version of the three-dimensional adaptive-grid model described in Skamarock and Klemp (1993). Like the model for the moist simulations, this model is fully compressible, nonhydrostatic, and three-dimensional. Although the model can be used with multiple grids, we use a single grid with a uniform horizontal resolution of 4 km. The horizontal domain is 600 km in x and 400 km in y, and the domain extends to a height of 16 km with a vertical resolution of 400 m. As in the moist simulations, upper and lateral boundaries are open to allow waves to propagate out of the computational domain with minimal spurious reflection. We chose a finer vertical resolution than WD98 to better resolve the low-level features, particularly the effect of the cooling. The slightly smaller horizontal domain and coarser resolution were chosen for computational efficiency. We performed sensitivity studies that indicate that varying the resolution from 2 to 4 km has very little effect on the results of the dry simulations.

The adaptive-grid model of Skamarock and Klemp (1993) is modified for the dry simulations. Potential temperature, θ, replaces virtual potential temperature, θ_v, in the momentum and pressure equations, and the thermodynamic energy equation becomes

$$\frac{d\theta}{dt} = D_\theta + Q,$$

where d/dt is the time derivative following a parcel, Q is the externally specified time mean thermal forcing, and D_θ denotes subgrid-scale mixing determined via a Richardson number–dependent first-order closure scheme (Durran and Klemp 1983).

b. Initial conditions

The simulations are initialized with the idealized thermodynamic sounding shown in Fig. 2a, which is meant

to represent typical conditions for strong midlatitude convection (Weisman and Klemp 1982). Two initial wind profiles are used: one with weak low-level shear and one with moderate low-level shear. These profiles are shown in Fig. 2b. The winds are shown in a reference frame moving with the mature storm. The initial environment is assumed to be horizontally homogeneous. As in WD98, when the Coriolis force is included in the simulations, a reference state with a horizontally uniform, geostrophically balanced pressure gradient is removed from the horizontal momentum equations, in which case the Coriolis force acts only on the perturbation velocity field. The time evolution of the reference state is neglected, although the reference state is only a perfectly steady solution of the governing equations when there is no vertical wind shear. Sensitivity tests, in which the model was integrated without any thermal perturbations, show that the circulations that develop in response to the lack of thermal wind balance associated with the low-level shear shown in Fig. 2b are small, a maximum of 6° of turning in the wind direction and a 5% perturbation in the wind speed over the 6-h time interval of the simulations. The acceptability of neglecting this small change in the mean wind is also supported by Skamarock et al. (1994b), who examined the evolution of numerically simulated squall lines in reference states that are exactly in thermal wind balance and found that they are not fundamentally different from those obtained using horizontally uniform basic states in which the Coriolis force acts only on the perturbation velocity field.

3. Overview of the simulations

We constructed two different steady thermal forcings: one from the weak-shear moist simulation of WD98 and one from the moderate-shear moist simulation of WD98. Both of these simulations were performed without Coriolis force. The shears in these two simulations are shown in Fig. 2b and encompass the range of environmental shears associated with multicellular systems.

The overall character of these simulations during their mature phase is shown in Figs. 3a, 3c, 4a, and 4c. The weak-shear moist simulation (Figs. 3a, 4a) shows a generally broad region of light precipitation extending rearward over the surface cold pool, with a narrow RIJ located between line-end vortices. The moderate-shear moist simulation (Figs. 3c, 4c) shows a stronger, more upright leading convective line with a stronger RIJ and stronger, larger line-end vortices. WD98 also performed a third moist simulation in an environment with deeper and stronger shear, but the convective system that developed in this shear was composed of cells that exhibited more supercellular characteristics.

The instantaneous heating and cooling produced by the microphysical processes in the moist simulations were diagnosed every 120 s. Time-mean storm-relative thermal forcings for each simulation were computed by averaging these values over a 2-h period in a coordinate frame moving with the leading edge of the convection. For the weak-shear simulation, the 2-h average was taken from 3 to 5 h. The time average was shifted back an hour for the moderate-shear simulation and computed over the period from 4 to 6 h to account for the slower evolution of the system in the moderate-shear environment. Time averaging emphasizes long timescale components of the forcing and eliminates the cellular signature of individual convective cells. Any residual cellularity was removed by smoothing the time-averaged forcing 20 times with a 2Δ smoother in x, y, and z. A single pass of this smoother along a single spatial coordinate has the form

$$Q_j^s = Q_j + \frac{1}{4}(Q_{j+1} - 2Q_j + Q_{j-1}),$$

where Q^s is the smoothed value and j is the gridpoint index.

Figure 3 compares the steady time-averaged thermal forcing with the instantaneous forcing in a horizontal plane 2 km above the ground. The shaded contours in Fig. 3a show the instantaneous pattern of heating and cooling at $t = 5$ h in the weak-shear moist simulation. The heating is concentrated in two arcs that are approximately tangent to each other at $x = 0$ km. The inner arc is associated with the main convective updraft, and the outer arc is caused by weak, shallow convection at the leading edge of the forward-spreading cold pool. Figure 3b shows the time-averaged thermal forcing derived from the weak-shear moist simulation, which is weaker and broader in x than the instantaneous forcing shown in Fig. 3a. As suggested by the differences between Figs. 3a and 3b, the 2-h time-averaged thermal forcing in the weak-shear simulation is not well approximated by the instantaneous forcing at any given time during the averaging period. On the other hand, the relation between the time-averaged thermal forcing and the instantaneous forcing at $t = 5$ h is much more obvious in the moderate shear simulations (cf. Figs. 3c and 3d).

The vertical structures of the instantaneous and time-averaged thermal forcings in the weak- and moderate-shear simulations are indicated in the line-averaged vertical cross sections in Figs. 4b and 4d, respectively. The line averages were taken over the region -35 km $< y < 35$ km. Only the envelopes of the heating and cooling regions are shown (by the ± 0.001 K s^{-1} contours). The shape of the line-averaged, time-averaged thermal forcings are generally similar to that deduced by Gallus and Johnson (1991) from observations of the 10–11 June Preliminary Regional Experiment for Storm-Scale Operational and Research Meteorology (PRE-STORM) squall line.

Note that the time-mean thermal forcings determined from the moist simulations show considerably more spatial structure than the simple heat sources used in most

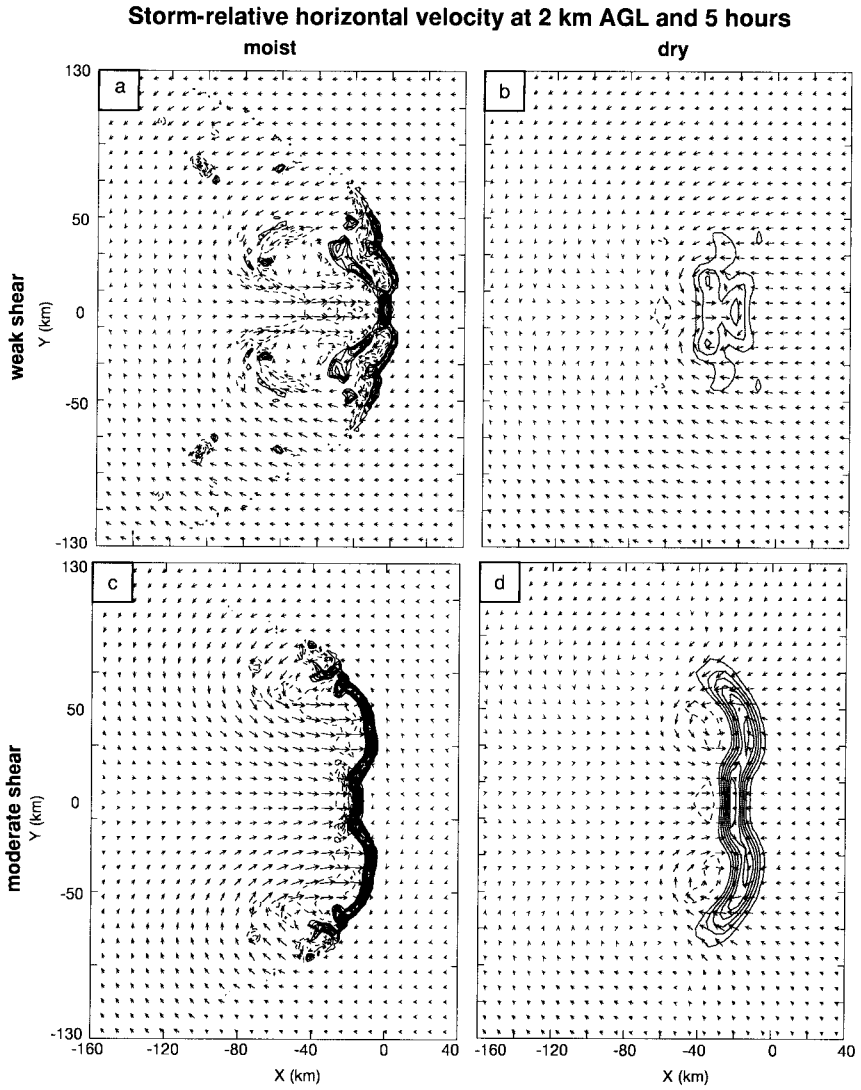

FIG. 3. (a) Storm-relative horizontal winds and instantaneous heating and cooling at 2 km AGL 5 h into the weak-shear moist simulation. Contour interval for heating and cooling is 0.004 K s^{-1}, with the zero contour omitted and negative values dashed. Dark (light) shading indicates heating (cooling) greater than 0.004 K s^{-1}. Vectors are plotted every 8 km; vector length of 8 km corresponds to wind speeds of ~21 m s^{-1}. (b) Storm-relative horizontal winds and steady thermal forcing at 2 km AGL 5 h into weak-shear dry simulation. Vectors as in (a); thermal forcing contour interval is 0.002 K s^{-1} with the zero contour omitted and negative values dashed. Dark (light) shading indicates heating (cooling) greater than 0.002 K s^{-1}. (c) As in (a), except for the moderate-shear moist simulation. (d) As in (b), except for the moderate-shear dry simulation.

previous studies in which the circulations within MCS are modeled as the response of a stratified fluid to a fixed heat source (e.g., Nicholls et al. 1991; Pandya et al. 1993; Mapes 1993). In particular, both the instantaneous and time-averaged forcing show a rearward tilt to the individual regions of heating and cooling and a displacement of the low-level cooling rearward from the region of maximum heating. On the basis of two-dimensional simulations, PD96 concluded that the tilt and the lateral displacement of the heating and cooling region are necessary to generate realistic circulations in the trailing stratiform region.

Storm-relative[1] horizontal wind vectors at 2 km above ground level (AGL) in the moist and dry simulations are also compared in Fig. 3. Figure 3b shows the winds

[1] Storm-relative winds in the dry simulations are the winds as viewed in the reference frame in which the thermal forcing is stationary.

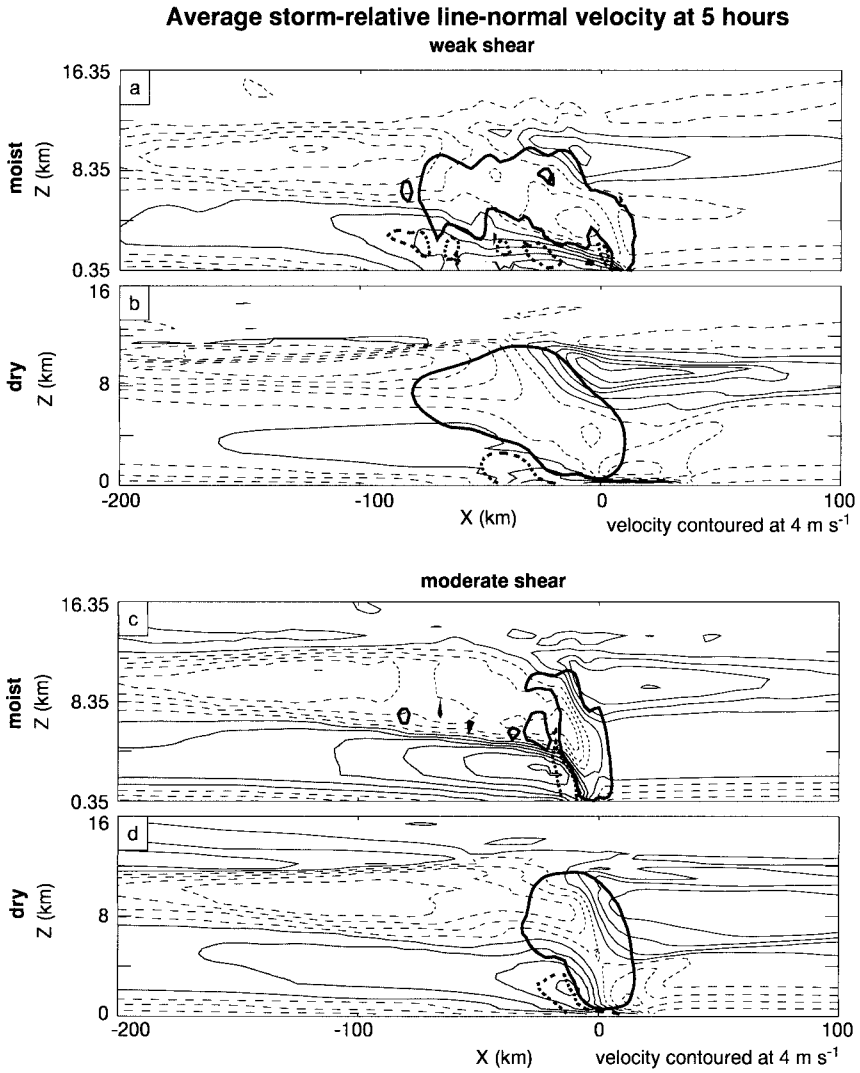

FIG. 4. (a) Along-line-averaged storm-relative line-normal velocity (thin lines) and the envelope of the instantaneous heating and cooling (thick lines) at 5 h in the weak-shear moist simulation. Velocity contour interval is 4 m s^{-1} with negative contours dashed and RIJ highlighted by shading. Instantaneous heating and cooling contours only at ± 0.001 K s^{-1} with negative contours dashed. (b) Along-line-averaged storm-relative winds (thin lines) at 5 h and envelope of the thermal forcing (thick lines) in the weak-shear dry simulation. Winds contoured as in (a); thermal forcing contoured as the instantaneous heating and cooling in (a). (c) As in (a), except for the moderate-shear moist simulation. (d) As in (c), except for the moderate-shear dry simulation.

in the weak-shear dry simulation, which was conducted using the weakly sheared environmental wind profile and the time-averaged thermal forcing diagnosed from the weak-shear moist simulation.[2] These winds may be compared with the instantaneous winds at $t = 5$ h from the weak-shear moist simulation shown in Fig. 3a. A similar comparison between the 2-km AGL wind in the moist and dry moderate-shear simulations is provided by Figs. 3c and 3d. (The moderate-shear dry simulation was conducted using the moderately sheared environmental wind profile and the time-averaged thermal forcing diagnosed from the moderate-shear moist simulation.) In all cases, the circulations include counterrotating line-end vortices and a strong RIJ between the vortices. The counterrotating vortices in the dry simulations qualitatively resemble the vortices in the corresponding moist simulations, although the vortices are weaker and closer together in the dry simulations.

In addition to the envelope of the heating and cooling

[2] The dry simulations were computed with the thermal forcings switched on instantaneously at time $t = 0$. We performed additional simulations in which the thermal forcing was switched on gradually, and we found that the evolution of the circulation was not significantly affected by the sudden start-up.

regions, Fig. 4 shows along-line-averaged vertical cross sections of the storm-relative winds in the moist and dry simulations. In all the simulations, the line-normal circulations include a strong RIJ, highlighted by shading, as well as an upper-level FTRF. The RIJ and FTRF are stronger in the moderate-shear simulations. The circulations in the moist and dry simulations are in general qualitative agreement, although the RIJ is weaker and less extensive in the dry simulations.

The comparisons shown in Figs. 3 and 4 indicate that appropriately specified steady thermal forcing can generate mesoscale circulations—such as the FTRF, RIJ, and the line-end vortices—that resemble the mesoscale circulations in the moist squall line simulations. Note that the dry simulations show the same shear-related variation in the circulation as the moist simulations. In the moderate-shear simulations, the RIJ is stronger and descends to the surface much closer to the leading line, the backward slant of the FTRF in the vicinity of the leading line is significantly smaller, and the line-end vortices are stronger, larger, and farther apart than in the weak-shear simulations.

The vertical shear in the environmental wind might be supposed to influence the storm structure in either of two ways: (1) by changing the strength and shape of the convection in the vicinity of the leading line, and thereby changing the time-mean thermal forcing (Garner and Thorpe 1992; Rotunno et al. 1988), or (2) by changing the environment through which the signals generated by a given thermal forcing propagate away from the convective region. The sensitivity of the storm to changes in the vertical shear that might arise via the second of these mechanisms was examined by performing a series of additional dry simulations. In these simulations the thermal forcing was fixed and the mean environmental winds were varied in order to determine the extent to which signals from identical thermal forcings propagating through differently sheared environments create different mesoscale circulations. These sensitivity tests demonstrated that the mesoscale circulation generated by a given thermal forcing is primarily determined by the shape and structure of the forcing and is relatively insensitive to the environmental wind shear. PD96 reported a similar result in their two-dimensional simulations. Thus, it appears that the shear-dependent variations in the circulation around real squall lines are primarily the result of the first mechanism described above, namely, the shear's influence on the shape, intensity, and orientation of the thermal forcing in the leading convective line.

4. Evolution of line-normal features

Several simplified models have shown that the mesoscale circulation surrounding a localized thermal forcing is established by the propagation of wave fronts away from the thermal forcing (Bretherton and Smolarkiewicz 1989; Nicholls et al. 1991; Mapes 1993; Pandya et al. 1993; Garner and Thorpe 1992; Pandya and Durran 1996). PD96 suggested that the circulation and thermodynamic features in the trailing stratiform region of two-dimensional squall lines are the result of gravity waves forced by the low-frequency component of the convective thermal forcing. In this section we seek to extend these conclusions to fully three-dimensional systems. We will examine only the evolution of the circulation in the weak-shear dry simulation; the evolution in the moderate-shear simulation is similar.

a. Line-normal circulation

Figure 5a shows the along-line-averaged x-component of the perturbation velocity in the weak-shear dry simulation at 1.5 h. As in Fig. 4 the velocity has been spatially averaged over the region $-35 \text{ km} < y < 35$ km to emphasize features that are uniform along the line. The perturbation velocity is shown instead of the total velocity in order to reveal features in the low-level flow that would otherwise be hidden in the strong low-level environmental winds. At 1.5 h, the back edge of the perturbation RIJ lies directly underneath the back edge of the FTRF at $x \sim -175$ km. The back edges of the RIJ and the FTRF remain vertically aligned as they propagate rearward and are still vertically aligned 2 h later, as shown in Fig. 5b. Garner and Thorpe (1992) and PD96 noted a similar vertical alignment of these features in their two-dimensional simulations.

Because the cold pool propagates rearward with speeds similar to the upper-level features, it is plausible that the propagation of the upper-level signal is dependent on the rearward-propagating cold pool. In order to test the relation of the cold pool's spread to that of the upper-level features, we performed an additional simulation in which the cold pool's rearward spread was inhibited by relaxing the low-level temperature perturbations back toward their initial values at every point more than 100 km behind the thermal forcing. The propagation of upper-level features was not affected in this simulation, even though the cold pool did not spread beyond $x = -100$ km. This suggests that rearward spread of the cold pool is not primarily responsible for the rearward propagation of the FTRF and RIJ.

In the absence of external forcing, the continued vertical alignment of the FTRF, RIJ, and low-level cold pool is suggestive of signal propagation via waves (Garner and Thorpe 1992; PD96). The signal (i.e., the rear edge of the FTRF, RIJ, and low-level cold pool) propagates rearward with a velocity of $\sim$19 m s^{-1}, which exceeds the rearward velocities behind the wave front in the FTRF and low-level cold pool, a clear indication that the signal is not advective. The speed of the signal corresponds to the horizontal phase and group speed of hydrostatic gravity waves with a vertical wavelength of 12 km, which is comparable to the depth of the thermal forcing. Another gravity wave signal with longer vertical wavelength is visible to the left of the FTRF and

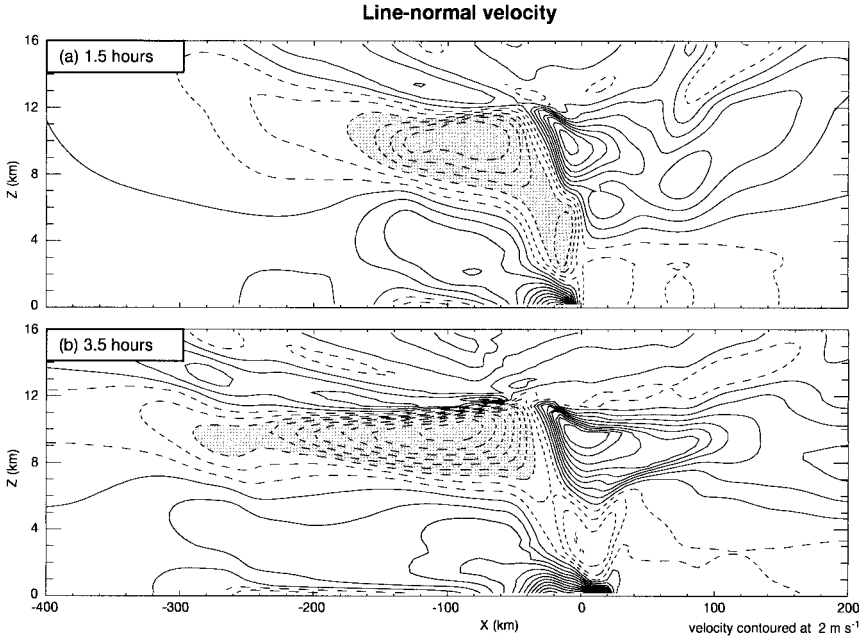

FIG. 5. Along-line-averaged line-normal perturbation velocity (thin lines, contour interval of 2 m s^{-1}) at (a) 1.5 and (b) 3.5 h into the weak-shear dry simulation. Rear inflow exceeding 2 m s^{-1} is lightly shaded and FTRF stronger than -6 m s^{-1} is darkly shaded.

RIJ in Fig. 5a; it is apparent as a weak front to rear flow extending to $x = -300$ km at $z \sim 15$ km. This mode has traveled out of the domain by the time of Fig. 5b. The dispersion of these two modes in Fig. 5 is reminiscent of the dispersion of vertical wavelengths in simplified linear models of a specified heating in a stratified fluid (Nicholls et al. 1991; Mapes 1993; Pandya et al. 1993) and is further evidence of the gravity wave character of the rearward propagation of the FTRF and RIJ.

b. The cold anvil

Figure 6, which shows the along-line-averaged perturbation potential temperature near the tropopause in the weak-shear dry simulation, reveals an extensive region of cooling at ~11 km AGL that extends rearward from $x = 0$ km. This upper-level cooling resembles the cloud-top cooling seen in both observations of LL-TS systems (Johnson et al. 1990; Gamache and Houze 1985; Ogura and Liou 1980) and in numerical models (Fritsch and Brown 1982). PD96 attributed a similar upper-tropospheric cooling in their two-dimensional simulations to adiabatic ascent within gravity waves generated in the leading convective line. The appearance of this cooling in the dry simulations shown here suggests that the upper-tropospheric cooling can be generated in response to a fully three-dimensional steady thermal forcing.

The gravity waves in and above the area of the cooling are particularly easy to recognize since these waves are largely monochromatic. The 90° phase shift between the potential temperature perturbations and the horizontal velocity perturbations (thin lines) in the region above 9 km AGL in Fig. 6 is characteristic of monochromatic

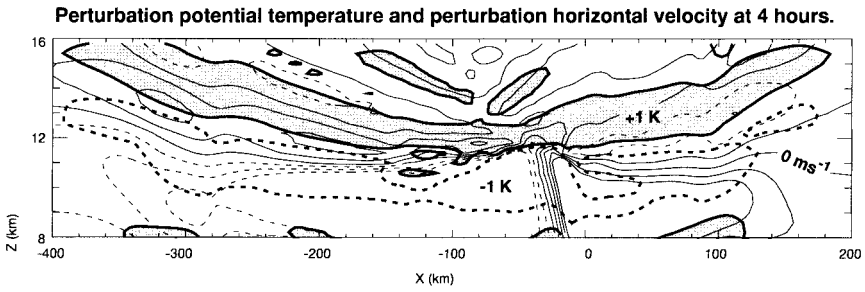

FIG. 6. Along-line-averaged line-normal perturbation velocity (thin lines, contour interval of 2 m s^{-1}) and perturbation potential temperature (dark shading for $\Delta\theta > 1$ K, light shading for $\Delta\theta < -1$ K) 4 h into the weak-shear dry simulation.

gravity waves. The slant of the velocity and potential temperature contours in the upper corners of the figure is consistent with gravity waves propagating energy away from the region of the thermal forcing. Thus, our three-dimensional simulations confirm that the upper-tropospheric cooling in the stratiform region of real squall lines can be generated as a gravity wave response to the time mean thermal forcing.

5. Formation of line-end vortices

As discussed in the introduction, the trailing stratiform region in real squall line systems contains significant three-dimensional circulations that can be classified into two broad categories: symmetric and asymmetric (Houze et al. 1990). Recent research indicates that asymmetric systems begin their life as symmetric systems (Scott and Rutledge 1995; Loehrer and Johnson 1995; Skamarock et al. 1994a; WD98; Hilgendorf and Johnson 1998). This section will investigate the influence of the latent heat released and absorbed in the vicinity of the leading convective line on the development of the three-dimensional circulations and line-end vortices in symmetric squall line systems. The evolution from symmetric to asymmetric systems will be discussed in more detail in section 6.

WD98 have suggested that the line-end vortices develop from the tilting of horizontal line-parallel vorticity. As illustrated in the schematic shown in Fig. 7, vortices of the correct sign (cyclonic to the north and anticyclonic to the south) can be generated by either localized ascent in a region of negative line-parallel vorticity (easterly shear) or localized descent in a region of positive line-parallel vorticity (westerly shear). In all the simulations presented here, the vorticity associated with the westerly shear in the mean wind is positive, and the only source of negative vorticity is the perturbed flow generated in response to the time mean thermal forcing. Thus, the two methods of forming vortices can be considered in terms the localized lifting of system-generated vorticity and the localized lowering of ambient vorticity.

An obvious way to determine the relative importance of these two mechanisms would be to vary only one of the vorticity sources at a time and examine the resulting line-end vortices. In moist simulations, however, this approach is impossible since the strength and structure of the convection, which influences the line-normal flow and hence the system-generated vorticity, is highly dependent on the environmental wind shear (Rotunno et al. 1988; Garner and Thorpe 1992). The dry simulations, on the other hand, decouple the thermal forcing and the implied system-generated vorticity from the ambient vorticity; changing the thermal forcing alone changes only the system-generated vorticity, while changing only the mean wind shear affects only the ambient vorticity (by definition). These simulations are not meant to be realistic simulations of squall line systems; rather, they are presented as sensitivity tests designed to determine the role of system-generated and ambient vorticity in the formation of line-end vortices.

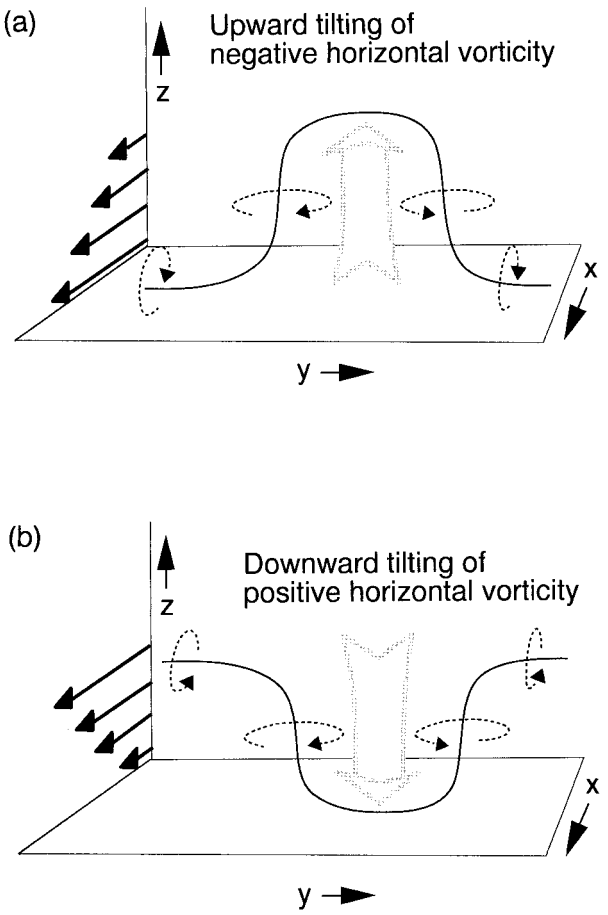

FIG. 7. Schematic of the vertical vorticity generation through vortex tilting. (a) For negative vorticity (easterly shear), ascending motion pushes the vortex lines up in the center, producing cyclonic rotation in the north and anticyclonic rotation in the south. (b) Localized descent in a region of positive vorticity (westerly shear) produces the same vertical vorticity pattern. (Adapted from Weisman and Davis 1998.)

Figure 8a shows the vortices that result from changing only the ambient vorticity. This simulation uses the same thermal forcing as the moderate-shear dry simulation (the envelope of the thermal forcing is indicated by the shading), but the environmental wind is vertically uniform. Thus, although the ambient vorticity is zero, the system-generated vorticity is largely unchanged from the moderate-shear dry simulation. The circulation in Fig. 8a can be compared to the circulation in the dry moderate-shear simulation (shown in Fig. 3d), which developed in the presence of both ambient and system-generated vorticity. Both simulations produce large-scale line-end vortices with a strong RIJ between them. The vortices in the absence of environmental wind shear are longer in the *y* direction, and they are located closer to the heating than the line-end vortices that form in the

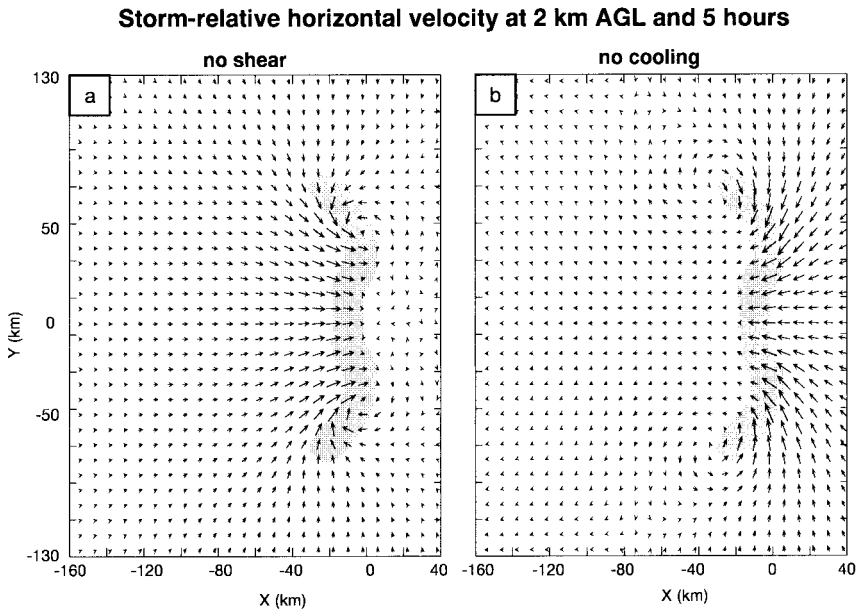

FIG. 8. Circulation at 2 km AGL 5 h into a simulation (a) identical to the moderate-shear dry simulation except that the environmental wind is uniform and (b) identical to the moderate-shear dry simulation except that the thermal forcing does not contain any cooling. Vectors and shading as in Fig. 3.

presence of environmental shear. Nevertheless, the similarity of the vortices in the two simulations suggests that changes in the ambient vorticity alone do not fundamentally alter the line-end vortices.

A second dry simulation was performed in order to test the influence of the system-generated vorticity on the formation of the line-end vortices. In this simulation the environmental winds are the same as those in the moderate-shear dry simulation, but only the positive part of the thermal forcing is used. Thus, the ambient vorticity is the same as in the moderate-shear dry simulation, but the system-generated vorticity is significantly different. We chose to modify the system-generated vorticity by eliminating the cold pool in order to highlight the importance of the cooling, which has been neglected in earlier studies (Lin 1986; Lin and Li 1988; Schubert et al. 1989; Fulton et al. 1995). The horizontal circulation generated without cooling is shown in Fig. 8b and bears little resemblance to the circulations in moderate-shear dry simulation (shown in Fig. 3d) or in real squall line systems. The vortices are in front of the leading line and the cyclonic vortex now appears at the south end of the line. The inability of the positive heating alone to produce line-end vortices of the correct sign shows that the production of these vortices is critically dependent on the shape and structure of the thermal forcing in the leading line, including, in particular, the low-level cooling.[3]

Our sensitivity tests demonstrate that the tilting of ambient vorticity by convective downdrafts does not contribute to the development of line-end vortices in moderately sheared environments. If ambient vorticity were advected downward deeper at the line's center then at the line ends, the resulting tilting of positive ambient vorticity would produce line-end vortices of the correct sign. If this mechanism were important to the production of line-end vortices, we would expect the simulations without shear to produce no vortices. Figure 8a, however, clearly shows that vortices are produced in the absence of shear.

In Fig. 9, we examine the line-parallel vorticity and vertical motion in x–z cross sections taken at $y = 0$ km in the dry simulations. Figure 9a shows the line-parallel vorticity (thin lines) and the vertical motion (thick lines) in the moderate-shear dry simulation. The main updraft is visible at $x = 0$ km. Negative line-parallel vorticity is highlighted by the shading; the negative vorticity is system-generated since the line-parallel vorticity associated with the environmental wind shear is positive. In Fig. 9a, the line-parallel vorticity in the region of the updraft is negative, resulting in the production of realistic vortices. (In all the cases shown in Fig. 9, the updrafts and line-parallel vorticity weaken away from the system's center. Thus, the tilting of the vorticity can be inferred from Fig. 9.) Figure 9b shows the line-parallel vorticity and vertical motion that develop from the same thermal forcing in the absence of the shear in the environmental wind. The line-parallel vorticity in the region of the updrafts is dominated by system-generated negative vorticity and, thus, lifting results in vortices of

[3] We also performed a simulation in which the environmental winds were uniform and the thermal forcing did not include cooling. Without either ambient or system-generated vorticity no line-end vortices of either sign develop.

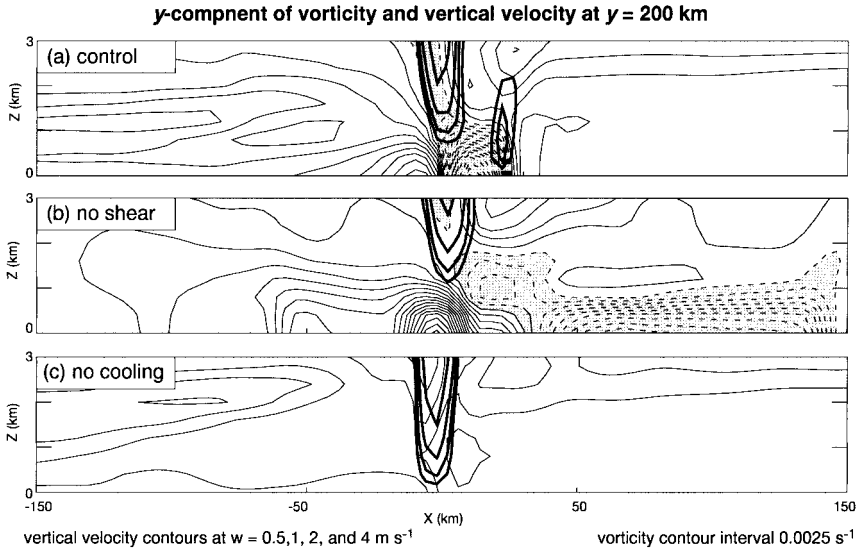

FIG. 9. The y component of the horizontal vorticity (thin lines, contour interval of 0.0025 s^{-1}, negative contours dashed) and the vertical velocity (thick lines, contours only at 0.5, 1, 2, and 4 m s^{-1}) at 5 h in (a) the moderate-shear dry simulation, (b) a simulation identical to the moderate-shear dry simulation except that the mean wind is uniform, and (c) a simulation identical to the moderate-shear simulation except that the thermal forcing has no cooling.

the correct sign. Note that the system-generated negative vorticity, which is associated with the negative buoyancy in the cold pool, has spread forward ahead of the line in the absence of an opposing low-level wind. The vorticity field in the absence of cooling (but with environmental shear) is shown in Fig. 9c. Notice that without the cooling, the low-level line-parallel vorticity field is uniformly positive, even in the region of upward vertical motion. This positive vorticity is the vorticity associated with the shear of the environmental wind. Lifting this positive vorticity in the central part of the leading line results in line-end vortices with the wrong sign.

We also tested the role of the ambient and system-generated vorticity in the line-end vortices that develop in the weak-shear case. Figure 10a shows the circulation that developed in a simulation identical to the weak-shear dry simulation except that the mean wind is uniform. As in the moderate-shear case the vortices are largely unaffected by the absence of wind shear, suggesting that the ambient vorticity associated with the environmental wind does not directly contribute to the formation of line-end vortices in squall line systems that develop in weak shear either. Figure 10b shows the circulation that develops in a dry simulation identical to the weak-shear dry simulation, except that the thermal forcing has been modified to remove the low-level cooling. In this simulation the only source of vertical vorticity is the tilting of the ambient vorticity due to the environmental wind shear, Fig. 10b reveals that the ambient vorticity is too weak to produce appreciable vortices of either sign when tilted.

Our simulations confirm the conclusion of WD98: that tilting of the system-generated, line-parallel horizontal vorticity produces the line-end vortices in squall line systems. Our simulations also underline the importance of the low-level cold pool in generating line-parallel vorticity at low levels of the correct sign to generate line-end vortices when tilted. These simulations also confirm that the tilting is accomplished in convective updrafts, not downdrafts. Although the vertical motions in the region of the applied thermal forcing are not easily described by gravity wave dynamics like the far-field motions discussed earlier, the formation of line-end vortices is nevertheless primarily the result of the time mean pattern of the latent heating and cooling in the leading convective line.

6. Influence of Coriolis force

As discussed earlier, real midlatitude squall lines evolve from symmetric to asymmetric organization (Loehrer and Johnson 1995; Hilgendorf and Johnson 1998). Two factors could contribute to asymmetries in the trailing stratiform anvil: a reorganization of the convective thermal forcing, or the influence of rotation on the communication between the convective and stratiform regions independent of changes in the convective line. In this section, we examine the influence of the Coriolis force on the circulation generated by the steady, symmetric thermal forcings already discussed. The use of a symmetric forcing allows us to isolate the effects of the Coriolis force on signal propagation through the fluid surrounding the leading convective line without allowing the reorganization of the convective line. In other words, we are trying to determine whether the action of the Coriolis force on the propagating wave

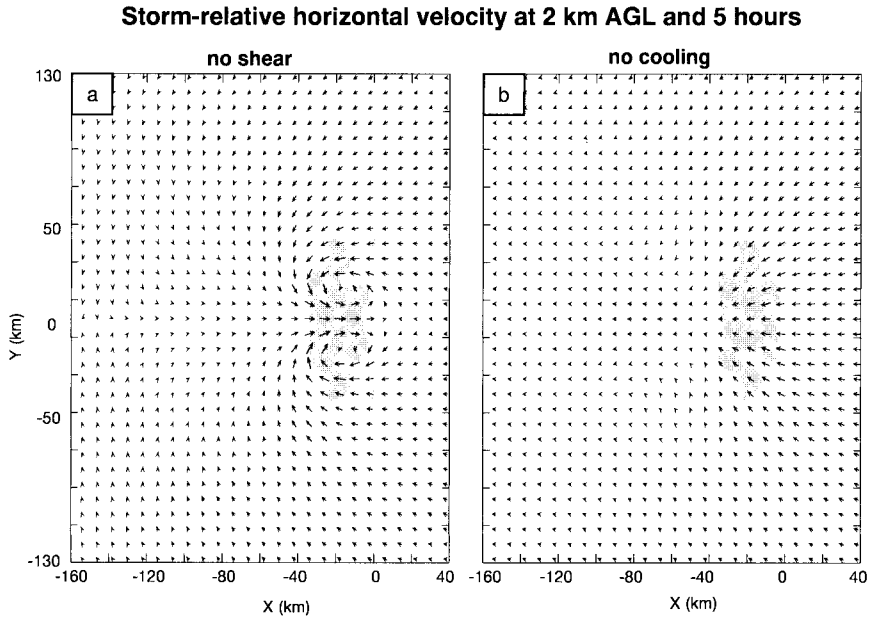

FIG. 10. Circulation at 2 km AGL 5 h into a simulation (a) identical to the weak-shear dry simulation except that the environmental wind is uniform and (b) identical to the weak-shear dry simulation except that the thermal forcing does not contain any cooling. Vectors and shading as in Fig. 3.

fronts is sufficient to generate asymmetries in the stratiform circulation or whether the asymmetries in the stratiform region reflect primarily asymmetries in the convective thermal forcing.

Figure 11a shows the circulation at 2 km AGL and 5 h generated by the symmetric thermal forcing shown in Fig. 3b in an environment with weak shear and a Coriolis parameter of 10^{-4} s^{-1}. Except for the Coriolis force, this simulation is identical to the dry weak-shear simulation. The circulation that develops under the in-

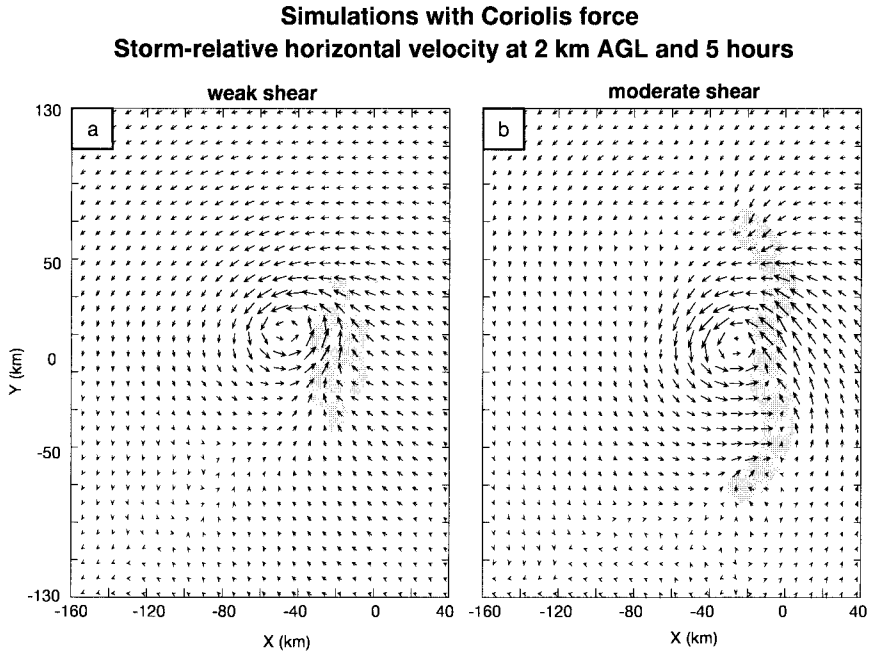

FIG. 11. Circulation at 2 km AGL 5 h into (a) the low-shear dry simulation with Coriolis force and (b) the moderate-shear dry simulation with Coriolis force. Vectors and contours as in Fig. 3.

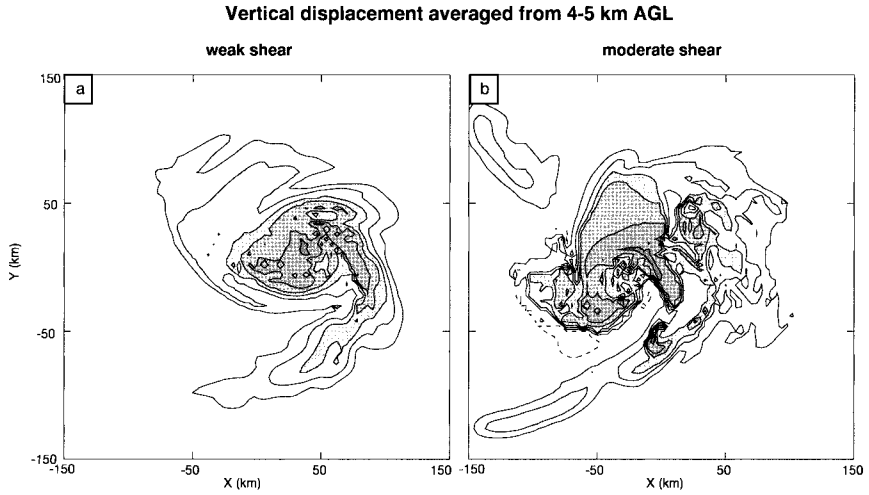

FIG. 12. Vertical displacement field averaged from 4 to 5 km AGL (contour interval of 1000 m, darkest shading for largest displacements) 6 h into (a) the weak-shear dry simulation with Coriolis force and (b) the moderate-shear dry simulation with Coriolis force.

fluence of the Coriolis force is dominated by a cyclonic vortex centered at $x = -40$ km and $y = 20$ km, which resembles the cyclonic vortex found in the stratiform region of real asymmetric squall line systems. Figure 11b shows the circulation at 2 km AGL and 5 h generated by the symmetric thermal forcing shown in Fig. 3d in a rotating environment with moderate shear. The midlevel circulation is dominated by a large cyclonic vortex just behind the leading convective line at $x = -10$ km. The vortex is centered behind the leading line and not located to the northwest of the line as in the conceptual model. Nevertheless, the response of a stably stratified rotating fluid to a steady symmetric thermal forcing qualitatively resembles the MCVs in real asymmetric squall line systems.

Under the influence of the Coriolis force the circulations in the dry simulations evolved from symmetric to asymmetric, just as in observations (Scott and Rutledge 1995; Loehrer and Johnson 1995; Hilgendorf and Johnson 1998) and moist simulations (Skamarock et al. 1994a; WD98). In both the weak- and moderate-shear simulations with and without the Coriolis force, the midlevel flow shows small nascent line-end vortices at early times. In simulations without the rotation, these vortices grow into larger line-end vortices. In the presence of rotation, the cyclonic vortex grows into the MCV while the anticyclonic vortex slowly dies. Analysis of the circulation in these simulations suggests that the cyclonic vortex is strengthened by convergence of planetary vorticity by convergent midlevel winds, as suggested by Skamarock et al. (1994a).

The trajectories of the air parcels within the FTRF (not shown) show a significant northward component and an anticyclonic character that are not present in the simulations performed in the absence of Coriolis force. This anticyclonic upper-level outflow resembles flow observed in real squall line systems (Houze et al. 1990) and in numerical simulations (Skamarock et al. 1994a). In real squall line systems, the advection of condensate to the north would result in a cloudy region to the north and west of the leading line. In the dry simulations there is no condensate. We can, however, look for areas where the parcels have undergone significant lifting over their lifetime to determine where the thermally forced circulation would favor the presence of condensate. Parcels that have undergone deep vertical lifting are likely to have come from the moist surface layer and been lifted enough to produce condensation; thus, areas with large vertical displacements indicate areas where the thermally forced circulation is likely to favor condensate. The vertical displacement field can be compared to observations of condensate in asymmetric squall line systems (e.g., Houze et al. 1990; Loehrer and Johnson 1995; Hilgendorf and Johnson 1998).

Figures 12a and 12b show the vertical displacement field averaged from 4 to 5 km AGL at 6 h in the weak- and moderate-shear dry simulations performed with Coriolis force. The vertical displacement of a parcel at a height z_f is determined by following the parcel's trajectory backward to its initial height z_0; the vertical displacement is then given by $z_f - z_0$. The largest vertical displacements are shaded the darkest in Figs. 12a and 12b. In both the weak- and moderate-shear simulations, the displacement field that develops under the influence of the Coriolis force shows a comma-shaped structure. Trajectories reveal the following history for these deeply lifted parcels: the air undergoes diabatically driven ascent in the region of the applied thermal forcing and is then advected away from the forcing in the gravity wave induced horizontal velocity perturbations. Under the influence of rotation, the upper- and midlevel outflow distribute the lifted air asymmetrically to form a

pattern similar to the comma-shaped cloud shield observed in real squall line systems.

7. Conclusions

We have examined the influence of the low-frequency thermal forcing occurring in the vicinity of the leading convective line on the three-dimensional meso-β-scale circulations within and surrounding squall line systems. We assessed the importance of the low-frequency thermal forcing by comparing the circulations that develop in pairs of moist and dry numerical simulations. The moist simulations were standard three-dimensional squall line simulations with parameterized microphysics. The dry simulations were conducted in identical atmospheric environments and were driven by steady regions of heating and cooling. These regions of heating and cooling were obtained by time averaging and spatially smoothing the instantaneous fields of thermal forcing generated by latent heating and cooling in the moist simulations.

Our results showed that the line-averaged line-normal circulations in the moist and dry simulations are fundamentally very similar. Analysis of the evolution of the circulations in the dry simulations reveals that the rearward spread of the RIJ and FTRF are associated with gravity wave propagation, of both linear and nonlinear waves. As noted previously in the two-dimensional studies of Nicholls et al. (1991), Pandya et al. (1993), and Mapes (1993), the tropospheric gravity wave response to a deep region of horizontally localized and steady thermal forcing bears little resemblance to simple monochromatic plane-parallel gravity waves but, rather, has a borelike structure whose leading edge remains aligned in the vertical. The wavelike character of the bore is confirmed by the fact that its leading edge propagates much faster than the winds just behind the wave front.

On the other hand, the thermally generated waves propagating near and above the tropopause are more nearly monochromatic, which allows individual wave modes to be identified using polarization relations. As in the two-dimensional study of PD96, a pronounced upper-tropospheric layer of cold air develops in both the moist and dry simulations, which resembles that observed in actual squall line systems (Ogura and Liou 1980; Gamache and Houze 1985). In the dry simulations, the source of this cooling can be unambiguously attributed to adiabatic cooling in air parcels displaced upward by gravity waves generated by the low-frequency components of the thermal forcing.

In addition to the diagnosis of prominent line-averaged features in our three-dimensional simulations, we also examined several of the most significant three-dimensional mesoscale circulations within the squall line system. The line-end vortices produced in the dry simulations were qualitatively similar to those obtained in the moist simulations, suggesting that these vortices are the nonlinear response of a stratified fluid to the time-averaged thermal forcing in the vicinity of the leading convective line. We also investigated the hypothesis of WD98 that the line-end vortices that develop in squall lines in weakly and moderately sheared environments are produced primarily by tilting system-generated line-parallel vorticity into the vertical, rather than through the tilting of line-parallel vorticity associated with the vertical shear in the environmental wind. The dry simulations provided a way to isolate these two possible sources of vorticity, since they allow the thermal forcing (and the resulting system-generated vorticity) to be varied independently of the environmental shear. Such sensitivity tests cannot be performed using moist numerical simulations because there is a strong interaction between the low-level environmental shear and the vertical motions and latent heat released in the leading convective line (Garner and Thorpe 1992; Rotunno et al. 1988).

These sensitivity tests confirm the results of WD98: the tilting of system-generated line-parallel vorticity is the primary source of vorticity for the line-end vortices, and it dominates the contribution due to the tilting of ambient vorticity associated with the environmental wind shear. Perhaps more importantly, these sensitivity tests also revealed that realistic line-end vortices could not be produced without including a region of low-level cooling in the thermal forcing. If the low-level cooling is neglected, no significant low-level system-generated vorticity develops, and the line-end vorticities produced by tilting the environmental vorticity have the wrong sign. These results emphasize the need to correctly include low-level cooling in convective parameterizations for large-scale models.

We examined the tendency of symmetric squall lines to develop asymmetric cloud shields and cyclonic MCVs in response to the Coriolis force. In observed squall lines (Loehrer and Johnson 1995; Hilgendorf and Johnson 1998) and moist squall line simulations (Skamarock et al. 1994a), the increasing asymmetry of an initially symmetric squall line system is accompanied by an increasing asymmetry in the shape of the leading convective line. The actual asymmetries that develop in those real-world squall lines that evolve from a relatively symmetric structure to a highly asymmetric form might be primarily due to the changing geometry of the leading convective line, or they might be largely due to the influence of the Coriolis force on signals propagating through a stably stratified fluid. In order to isolate the influence of the Coriolis force on signal propagation from those effects due to changes in the geometry of the thermal forcing, we performed additional dry simulations in which the circulations generated by the previously considered symmetric thermal forcings were subject to the Coriolis force. We only considered the evolution of the squall line over the first 5 h of its development. Since our computations are based on simulations with a fixed heat source representative of a relatively early phase of the squall line life cycle, the

ultimate approach of the system toward a geostrophically balanced steady state is beyond the scope of this study. [See Schubert et al. (1989) or Fulton et al. (1995) for a discussion of the permanent modification induced by a squall line in the large-scale balanced flow.]

In the presence of the Coriolis force, symmetric thermal forcing generated circulations that included an MCV roughly resembling those in asymmetric squall line systems. The evolution of the MCV mimicked observations and mesoscale squall line simulations in that the initial line-end vortices evolved into a single cyclonic vortex. In addition, the air parcels that experienced large upward displacements were distributed in a comma-shaped pattern resembling that observed in the stratiform anvils associated with many midlatitude squall lines. The vertical displacement field provides the best proxy data from which to estimate a cloud pattern in the dry simulations, and its realistic appearance suggests that the asymmetries that evolve in real squall lines need not be exclusively the result of asymmetries in the thermal forcing along the leading line.

Acknowledgments. Support for REP is provided by the Advanced Study Program at the National Center for Atmospheric Research. DRD's research was supported by NSF Grant ATM-9530662. The authors would like to thank Drs. C. Davis, R. Rotunno, and B. Skamarock for their comments that significantly improved the manuscript. We would also like to thank the anonymous reviewers who provided significant guidance in revising the manuscript.

REFERENCES

Braun, S. A., R. A. Houze Jr., and M.-J. Yang, 1996: Comments on ''The impact of the ice phase and radiation on a midlatitude squall line system.'' *J. Atmos. Sci.,* **53,** 1343–1351.

Bretherton, C. S., 1988: Group velocity and the linear response of stratified fluids to internal heat or mass sources. *J. Atmos. Sci.,* **45,** 81–93.

——, and P. K. Smolarkiewicz, 1989: Gravity waves, compensating subsidence, and detrainment around cumulus clouds. *J. Atmos. Sci.,* **46,** 740–759.

Cram, J. M., R. A. Pielke, and W. R. Cotton, 1992: Numerical simulation and analysis of a prefrontal squall line. Part II: Propagation of the squall line as an internal gravity wave. *J. Atmos. Sci.,* **49,** 209–225.

Durran, D. R., and J. B. Klemp, 1983: A compressible model for the simulation of moist mountain waves. *Mon. Wea. Rev.,* **111,** 2341–2361.

Fovell, R. G., and Y. Ogura, 1988: Numerical simulation of a midlatitude squall line in two dimensions. *J. Atmos. Sci.,* **45,** 3846–3879.

Fritsch, J. M., and J. M. Brown, 1982: On the generation of convectively driven mesohighs aloft. *Mon. Wea. Rev.,* **110,** 1554–1563.

Fulton, S. R., W. H. Schubert, and S. A. Hausman, 1995: Dynamical adjustment of mesoscale convective anvils. *Mon. Wea. Rev.,* **123,** 3215–3226.

Gallus, W. A., Jr., and R. H. Johnson, 1991: Heat and moisture budgets in an intense midlatitude squall line. *J. Atmos. Sci.,* **48,** 122–146.

Gamache, J. F., and R. A. Houze Jr., 1985: Further analysis of the composite wind and thermodynamic structure of the 12 September GATE squall line. *Mon. Wea. Rev.,* **113,** 1241–1259.

Garner, S. T., and A. J. Thorpe, 1992: The development of organized convection in a simplified squall line model. *Quart. J. Roy. Meteor. Soc.,* **118,** 101–124.

Hilgendorf, E. R., and R. H. Johnson, 1998: A study of the evolution of mesoscale convective systems using WSR-88D data. *Wea. Forecasting,* **13,** 437–452.

Houze, R. A., Jr., 1989: Observed structure of mesoscale convective heating and implications for large-scale heating. *Quart. J. Roy. Meteor. Soc.,* **115,** 425–461.

——, 1993: *Cloud Dynamics.* Academic Press, 570 pp.

——, B. F. Smull, and P. Dodge, 1990: Mesoscale organization of springtime rainstorms in Oklahoma. *Mon. Wea. Rev.,* **118,** 613–654.

Jorgenson, D. P., and B. F. Smull, 1993: Mesovortex circulations seen by airborne Doppler radar within a bow-eco mesoscale convective system. *Bull. Amer. Meteor. Soc.,* **74,** 2146–2157.

Klemp, J. B., and R. B. Wilhelmson, 1978: The simulation of three-dimensional convective storm dynamics. *J. Atmos. Sci.,* **35,** 1070–1096.

Klimowski, B. A., 1994: Initiation and development of rear inflow within the 28–29 June 1989 North Dakota mesoconvective system. *Mon. Wea. Rev.,* **122,** 765–779.

Lafore, J.-P., and M. W. Moncrieff, 1989: A numerical investigation of the organization and interaction of the convective and stratiform regions of tropical squall lines. *J. Atmos. Sci.,* **46,** 521–544.

LeMone, M. A., 1983: Momentum transport by a line of cumulonimbus. *J. Atmos. Sci.,* **40,** 1815–1834.

Lin, Y. L., 1986: Circulation of airflow over an isolated heat source with application to the dynamics of V-shaped clouds. *J. Atmos. Sci.,* **43,** 2736–2751.

——, and R. B. Smith, 1986: Transient dynamics of airflow near a local heat source. *J. Atmos. Sci.,* **43,** 40–49.

——, and S. Li, 1988: Three-dimensional response of a shear flow to elevated heating. *J. Atmos. Sci.,* **45,** 2987–3002.

Loehrer, S. M., and R. H. Johnson, 1995: Surface pressure and precipitation life cycle characteristics of PRE-STORM mesoscale convective systems. *Mon. Wea. Rev.,* **123,** 600–621.

Mapes, B. E., 1993: Gregarious tropical convection. *J. Atmos. Sci.,* **50,** 2026–2037.

McAnelly, R. L., J. A. Nachamkin, W. R. Cotton, and M. E. Nicholls, 1997: Upscale evolution of MCSs: Doppler radar analysis and analytical investigation. *Mon. Wea. Rev.,* **125,** 1083–1110.

Nicholls, M. E., R. A. Pielke, and W. R. Cotton, 1991: Thermally forced gravity waves in an atmosphere at rest. *J. Atmos. Sci.,* **48,** 1869–1884.

Ogura, Y., and M.-T. Liou, 1980: The structure of a midlatitude squall line: A case study. *J. Atmos. Sci.,* **37,** 553–567.

Pandya, R. E., and D. R. Durran, 1996: The influence of convectively generated thermal forcing on the mesoscale circulation around squall lines. *J. Atmos. Sci.,* **53,** 2924–2951.

——, ——, and C. Bretherton, 1993: Comments on ''Thermally forced gravity waves in an atmosphere at rest.'' *J. Atmos. Sci.,* **50,** 4097–4101.

Rotunno, R., J. B. Klemp, and M. L. Weisman, 1988: A theory for long-lived squall lines. *J. Atmos. Sci.,* **45,** 463–485.

Schmidt, J. M., and W. R. Cotton, 1989: A High Plains squall line associated with severe surface winds. *J. Atmos. Sci.,* **46,** 281–302.

——, and ——, 1990: Interactions between upper and lower tropospheric gravity waves on squall line structure and maintenance. *J. Atmos. Sci.,* **47,** 1205–1222.

Schubert, W. H., S. R. Fulton, and R. F. A. Hertenstein, 1989: Balanced atmospheric response to squall lines. *J. Atmos. Sci.,* **46,** 2478–2483.

Scott, J. D., and S. A. Rutledge, 1995: Doppler radar observations of an asymmetric mesoscale convective system and associated vortex couplet. *Mon. Wea. Rev.,* **123,** 3437–3457.

Skamarock, W. C., J. B. Klemp, 1993: Adaptive grid refinement for two-dimensional and three-dimensional nonhydrostatic atmospheric flow. *Mon. Wea. Rev.,* **121,** 788–804.

——, M. L. Weisman, and J. B. Klemp, 1994a: Three-dimensional evolution of simulated long-lived squall lines. *J. Atmos. Sci.,* **51,** 2563–2584.

——, ——, C. A. Davis, and J. B. Klemp, 1994b: The evolution of simulated mesoscale convective systems in idealized environments. Preprints, *Sixth Conf. on Mesoscale Processes,* Portland, OR, Amer. Meteor. Soc., 407–410.

Smith, R. B., and Y. L. Lin, 1982: The addition of heat to a stratified airstream with application to the dynamics of orographic rain. *Quart. J. Roy. Meteor. Soc.,* **108,** 353–378.

Smull, B. F., and R. A. Houze Jr., 1985: A midlatitude squall line with a trailing region of stratiform rain: Radar and satellite observations. *Mon. Wea. Rev.,* **113,** 117–133.

——, and ——, 1987: Rear inflow in squall lines with trailing stratiform precipitation. *Mon. Wea. Rev.,* **115,** 2869–2889.

Tripoli, G., and W. R. Cotton, 1989: Numerical study of an observed orographic mesoscale convective system. Part II: Analysis of the governing dynamics. *Mon. Wea. Rev.,* **117,** 305–328.

Weisman, M. L., 1992: The role of convectively generated rear-inflow jets in the evolution of long-lived mesoconvective systems. *J. Atmos. Sci.,* **49,** 1826–1847.

——, and J. B. Klemp, 1982: The dependence of numerically simulated convective storms on vertical wind shear and buoyancy. *Mon. Wea. Rev.,* **110,** 504–520.

——, and C. A. Davis, 1998: Mechanisms for the generation of mesoscale vortices within quasi-linear convective systems. *J. Atmos. Sci.,* **55,** 2603–2622.

Yang, M.-J., and R. A. Houze Jr., 1995a: Multicell squall-line structure as a manifestation of vertically trapped gravity waves. *Mon. Wea. Rev.,* **123,** 641–661.

——, and ——, 1995b: Sensitivity of squall-line rear inflow to ice microphysics and environmental humidity. *Mon. Wea. Rev.,* **123,** 3175–3193.

Zipser, E. J., 1977: Mesoscale and convective-scale downdrafts as distinct components of squall-line structure. *Mon. Wea. Rev.,* **105,** 1568–1589.